IX International Conference on Computational Methods in Marine Engineering
MARINE 2021
I.M. Viola and F. Brennan (Eds)

PREDICTION MODEL FOR PARTIALLY CAVITATING HYDROFOILS BASED ON SENSITIVITY DERIVATIVES

D. ANEVLAVI[*] AND K.A. BELIBASSAKIS [†]

[*] School of Naval Architecture and Marine Engineering (NTUA)
National Technical University of Athens, Greece
NTUA Campus, 15780 Athens, Greece
E-mail: danevlavi@mail.ntua.gr, web page: https://sites.google.com/view/dimitraanevlavi

[†] School of Naval Architecture and Marine Engineering (NTUA)
National Technical University of Athens, Greece
NTUA Campus, 15780 Athens, Greece
E-mail: kbel@fluid.mech.ntua.gr, web page: http://arion.naval.ntua.gr/~kbel/

Key words: Cavitation, Adjoint Method, Sensitivity Derivatives, Boundary Element Method

Abstract. Much work has been done over the past years to obtain a better understanding of cavitation, as well as to predict and alleviate its effects on performance. Particularly, lifting-surface sheet cavitation is addressed in various works as a free-streamline problem. Typically, a potential solver is used in conjunction with a geometric criterion to determine the shape of the cavity, whereas an iterative scheme is employed to locate the cavity surface. In this work we reformulate the problem of steady partially cavitating two-dimensional hydrofoils in a shape-optimization setup. The sensitivities required for the gradient-based optimization algorithm are derived using the continuous adjoint method. The objective function is formulated based on the assumption that the pressure on the cavity is constant and is evaluated using a source-vorticity BEM solver, whereas the control points of the B-spline cavity parametrization serve as design variables. The proposed numerical scheme is validated and found to predict well both the cavity shape and the cavitation number. Moreover, the benefits of using the adjoint method to predict the sensitivity derivatives are highlighted in a selected study case.

1 INTRODUCTION

One of the most severe technical requirements imposed on the design of lifting surfaces for hydrokinetic turbines and marine propulsion systems is due to cavitation. Many forms of cavitation exist, such as bubble cavitation, cloud cavitation and sheet cavitation. As it develops, cavitation creates noise, vibration, metal erosion and, finally, a drop in performance. [1].

In this work we address the problem of hydrofoil cavitation as a free streamline problem. In formulations as such, a potential solver is used in conjunction with a geometric criterion to determine the shape of the cavity, whereas an iterative scheme is employed to locate the cavity surface [2,3]. Upon convergence the exact boundary conditions are satisfied on all portions of the foil-cavity boundary. However, non-iterative methods have also been considered; see [4]. Particularly shape optimization techniques based on the adjoint method

were employed to determine the optimum (minimum-drag) shape of a supercavitating torpedo given certain operating conditions; see [5,6]. The developed methodology consists of an optimization process able to determine the cavity and cavitator shapes simultaneously.

The adjoint method is increasingly gaining popularity in the field of multidisciplinary optimization for it requires less evaluations than any evolutionary algorithm in problems where the number of design variables is greater than the number cost functions [5]. The discrete version of the adjoint method has also been implemented in the design of vessel hulls [7], with an excellent comparison between the sensitivities obtained with the adjoint method and the reference values corresponding to finite-differences. Motivated by these results, in this work we reformulate the problem of steady partially cavitating two-dimensional hydrofoils in a shape-optimization setup. The sensitivities required for the gradient-based optimization algorithm are derived using the continuous adjoint method; see also [8,9]. The sensitivities can also be derived using symbolic mathematics to further facilitate the process, as presented in [10]. The objective function is based on the assumption that the pressure on the cavity remains constant, and is evaluated at each optimization cycle using a source-vorticity BEM solver; see [11]. In terms of the cavity shape, the control points of the B-spline cavity parametrization are included in the set of design variables.

Finally, regarding the problem statement and the targeted unknowns, we address two variations. The first is namely the cavity shape prediction for fixed cavity length and unknown cavitation number; as presented in [2]. The second, more challenging, is known as the `direct problem' and consists of determining the cavity extent, as well as the cavity shape for given cavitation number; see [3].

The proposed numerical scheme is compared with other methods, in terms of the first problem statement and is found to predict well the cavity shape and the cavitation number. Moreover, the benefits of using the adjoint method to predict the sensitivity derivatives, instead of the standard finite difference scheme, are highlighted in a study case.

2 OPTIMIZATION PROBLEM

The geometry of the hydrofoil is represented as a clock-wise directional closed parametric curve,

$$C := \mathbf{r}(t) = \{(x,y) \in \mathbb{R}^2 : x = x(t), y = y(t), t \in I\}. \tag{1}$$

with $x(t_o) = x(t_1), y(t_o) = y(t_1)$ denoting the trailing edge, and can be remodeled for any given set of nodal coordinates using B-spline interpolation. The control points that affect the shape of the cavity boundary Γ_c are included in the set of design variables $b_n, n = \{1,\ldots,N\}$. The detachment and termination points of the constant-pressure cavity surface are denoted as s_D, s_T respectively, whereas s_L is the re-attachment point. Finally the dot notation $\dot{r}(t)$ denotes differentiation with respect to the curve parameter t.

In this work, the lifting-surface sheet cavitation problem is addressed as a free streamline problem and thus the cavity surface is to be determined upon the solution to the following shape-optimization problem. On the cavity boundary $\Gamma_c = \{(x,y) \in \mathbb{R}^2 : t \in (t_D, t_T)\}$ we assume that the cavitation number is constant, consequently the pressure is assumed uniform. To translate this into a cost functional,

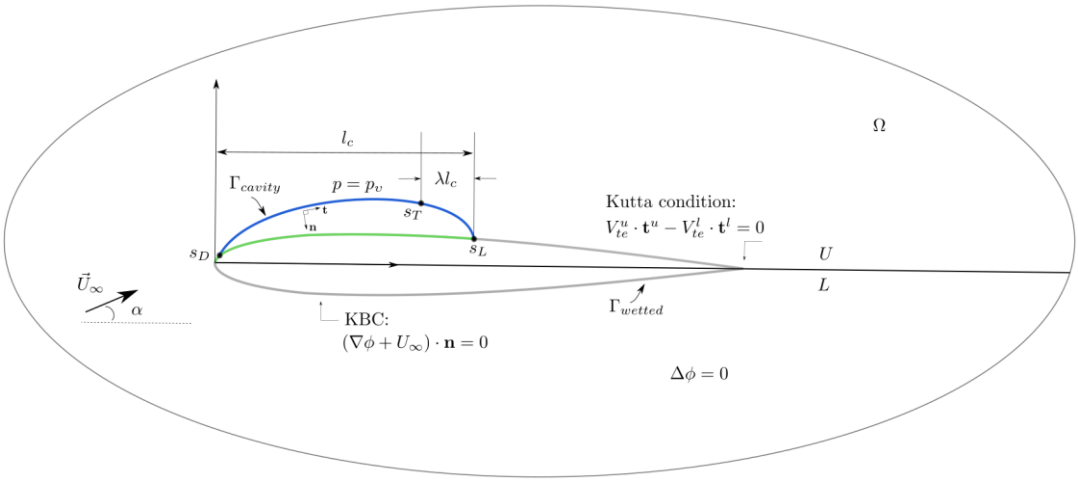

Figure 1. Problem formulation for 2d partially cavitating foil in steady flow.

$$F = \int_{\Gamma_c} g ds = \int_{\Gamma_c} \frac{1}{2} \left(p - p_v \right)^2 ds, \tag{2}$$

where p_v is the target cavity pressure. The cavitation number is defined as

$$\sigma = \frac{p_\infty - p_v(\mathrm{T}_\infty)}{0.5\rho U_\infty^2}, \tag{3}$$

where U_∞, p_∞ and T_∞ are respectively a reference velocity, pressure and temperature in the flow (usually upstream quantities), ρ the density of the fluid and $p_v(\mathrm{T}_\infty)$ is the saturated vapor pressure. Particularly, the kernel of the objective function can also be expressed in terms of the non-dimensional pressure coefficient $(C_p = 0.5\rho U_\infty^2)$ as follows

$$p - p_v = 0.5\rho U_\infty^2 \left(C_p + \sigma \right). \tag{4}$$

Notably, admissible solutions must comply with the requirements of incompressible, inviscid and irrotational fluid motion in the region. The primal problem in terms of the disturbance velocity potential $\varphi(x, y; b_n)$ serves as a constraint and is stated as

$$R = R\left(\varphi(x, y; b_n), b_n \right) = \nabla^2 \varphi = 0, \quad (x, y) \in \Omega, \tag{5}$$

$$R_{Kutta} = \left(\nabla\varphi + U_\infty \right) \cdot \mathbf{t}\Big|_{t_o} + \left(\nabla\varphi + U_\infty \right) \cdot \mathbf{t}\Big|_{t_1} = 0, \tag{6}$$

with boundary conditions

$$\frac{\partial \Phi}{\partial n} = \left(\nabla\varphi + U_\infty \right) \cdot \mathbf{n} = 0, \quad (x, y) \in \Gamma = \Gamma_c \cup \Gamma_{wetted}, \tag{7}$$

$$\nabla\varphi = 0, \quad (x,y) \to \infty, \tag{8}$$

where $\nabla\varphi$ denotes the disturbance velocity, Φ the total potential, **n** and **t** the normal (directed inwards) and tangential vector, respectively; see Figure 1. The boundary value problem presented above can be solved when the ambient free-stream flow and the boundary of the hydrofoil are known. After the velocity potential has been determined the pressure can be evaluated using Bernoulli's theorem for steady potential flows

$$p + \frac{1}{2}\rho V^2 = p_\infty + \frac{1}{2}\rho U_\infty^2 = c_\infty. \tag{9}$$

Finally, it is important to note that the primal variable is assumed to be implicitly dependent on the design variables. In literature several variations of the partial cavitation problem can be found [2, 3]. In the scope of the present work, the following variation is considered, whereas other variations are left to be examined in future work

- Determine the cavity shape and cavitation number $b_n = \sigma, x_i, y_i, \ldots, \lambda_{TL}$ based on known cavity length l_c / c. The design variables consist of the cavitation number, the coordinates of the B-spline parametrization of the attached cavity, as well as the length of the pressure attenuation region λ_{TL}.

2.1 Sensitivity derivatives

In this work the simple steepest-descend method is implemented to treat numerically the deterministic optimization problem. The straightforward approach would be to calculate the derivatives of the objective function with respect to the design variables by implementing a central difference scheme

$$\frac{dF}{db_n} \approx \frac{F\ x,y;b_n + h\ - F\ x,y;b_n - h}{2h}. \tag{10}$$

However, this approach requires $2N$ evaluations of the primal problem, with N denoting the total number of design variables. As an alternative we propose the use of the continuous adjoint method to produce estimates of the sensitivity derivatives that require fewer evaluations of the primal problem; particularly two evaluations per optimization cycle. The adjoint-state equations are derived along with the sensitivity derivatives by introducing the adjoint velocity potential ψ as a Lagrange multiplier. The derivation for the continuous adjoint method occurs at the level of the partial differential equations. Note that the primal problem in Eq. (5) holds for every $(x,y) \in \Omega$, therefore the integral term is zero. The augmented cost functional is

$$L = F + \iint_\Omega \psi R\ \delta\Omega + \int_\Gamma \psi\delta\ s - s_o\ R_{Kutta}\ ds, \tag{11}$$

with $\delta\ s-s_o\ $ denoting the Dirac delta generalized function. In order to obtain the sensitivity derivatives we take the first variation of the functional, see [12], with respect to the design variables $b_n, n=\{1,\ldots,N\}$ as follows

$$\frac{\delta L}{\delta b_n}=\frac{\delta}{\delta b_n}\int_{\Gamma_c}\frac{1}{2}\ p-p_v\ ^2\,ds+\frac{\delta}{\delta b_n}\iint_{\Omega}\psi R\ \delta\Omega+\frac{\delta}{\delta b_n}\int_{\Gamma}\psi\delta\ s-s_o\ \ R_{Kutta}\ ds. \tag{12}$$

2.2 Variation of the objective functional

The first term in Eq. (12) has to be differentiated as follows

$$\frac{\delta F}{\delta b_n}=g(s_T)\frac{\delta s_T}{\delta b_n}-g(s_D)\frac{\delta s_D}{\delta b_n}+\int_{s_D}^{s_T}\frac{\delta g}{\delta b_n}ds+\int_{s_D}^{s_T}g\frac{\delta(ds)}{\delta b_n}, \tag{13}$$

where $s_D=\int_{t_o}^{t_D}\|\dot{\mathbf{r}}\|dt,\ s_T=\int_{t_o}^{t_T}\|\dot{\mathbf{r}}\|dt$ with $\{t_o,t_D,t_T\}\in I$. The first two terms in Eq. (13) appear after the implementation of the Leibnitz rule of integration. The differentiated form of the cost functional is therefore,

$$\begin{aligned}\frac{\delta F}{\delta b_n}=&\int_{s_D}^{s_T}-\rho V_t\ \ p-p_v\ \ \nabla_s\left(\frac{\delta\varphi}{\delta b_n}\right)ds-\int_{s_D}^{s_T}\ p-p_v\ \ \frac{\delta p_v}{\delta b_n}ds\\&+\int_{s_D}^{s_T}-\rho V_t\ \ p-p_v\ \ \ \nabla\varphi+\mathbf{U}_\infty\ \cdot\frac{\delta\mathbf{t}}{\delta b_n}dt+g(s_T)\frac{\delta s_T}{\delta b_n}-g(s_D)\frac{\delta s_D}{\delta b_n}+\int_{t_D}^{t_T}g\frac{\delta\|\dot{\mathbf{r}}\|}{\delta b_n}dt\end{aligned} \tag{14}$$

Note that, it is not possible to explicitly determine the derivative term $\delta\varphi/\delta b_n$, since the velocity potential φ is implicitly dependent on the design variables.

2.3 Variation of constraints

Using the Gauss theorem along with the no-entry boundary condition Eq. (7), the second term in Eq. (12) becomes

$$\frac{\delta}{\delta b_n}\iint_{\Omega}\psi R\ d\Omega=\iint_{\Omega}\frac{\delta\varphi}{\delta b_n}\cdot\Delta\psi\ d\Omega+\int_{\Gamma}\frac{\delta\varphi}{\delta b_n}\nabla\psi\cdot\mathbf{n}\ ds\ -\int_{\Gamma}\psi\ \ \nabla\varphi+\mathbf{U}_\infty\ \cdot\frac{\delta\mathbf{n}}{\delta b_n}\ ds. \tag{15}$$

The third term in Eq. (12) imposing a stagnation point at the trailing edge becomes

$$\frac{\delta R_{Kutta}}{\delta b_n}=\frac{\delta\ \nabla\varphi\ _o}{\delta b_n}\mathbf{t}_o+\frac{\delta\ \nabla\varphi\ _1}{\delta b_n}\cdot\mathbf{t}_1, \tag{16}$$

taking into account the discontinuity of the velocity disturbance potential at the vicinity of the trailing edge. The tangential vectors near the trailing edge are not dependent on the design variables and therefore $\delta\mathbf{t}_o/\delta b_n=\delta\mathbf{t}_1/\delta b_n=0$.

2.4 Adjoint problem and sensitivities

The first variation of the augmented objective function is derived from Eqs. (12-16), after re-arranging terms and using integration by parts,

$$\frac{\delta L}{\delta b_n} = SD + \int_{s_D}^{s_T} \rho \nabla_s \; V_t(p - p_v) \; \frac{\delta \varphi}{\delta b_n} ds + \iint_{\Omega} \frac{\delta \varphi}{\delta b_n} \cdot \Delta \psi \; d\Omega + \int_{\Gamma} \frac{\delta \varphi}{\delta b_n} \nabla \psi \cdot \mathbf{n} \tag{17}$$

$$- \left[\rho V_t (p - p_v) \frac{\delta \varphi}{\delta b_n} \right]_{s_D}^{s_T} + \psi(s_o) \frac{\delta \; \nabla \varphi \; _o}{\delta b_n} \mathbf{t}_o + \psi(s_1) \frac{\delta \; \nabla \varphi \; _1}{\delta b_n} \cdot \mathbf{t}_1,$$

where

$$SD = \int_{s_D}^{s_T} -\rho V_t \;\; p - p_v \;\; \nabla \varphi + \mathbf{U}_\infty \;\; \cdot \frac{\delta \mathbf{t}}{\delta b_n} \| \dot{\mathbf{r}} \| ds - \int_{s_D}^{s_T} \;\; p - p_v \;\; \frac{\delta p_v}{\delta b_n} ds \tag{18}$$

$$+ g(s_T) \frac{\delta s_T}{\delta b_n} - g(s_D) \frac{\delta s_D}{\delta b_n} + \int_{t_D}^{t_T} g \frac{\delta \| \dot{\mathbf{r}} \|}{\delta b_n} dt - \int_{\Gamma} \psi \;\; \nabla \varphi + \mathbf{U}_\infty \;\; \cdot \frac{\delta \mathbf{n}}{\delta b_n} ds,$$

serves as the approximation formula for the sensitivity derivatives. The adjoint boundary value problem is introduced so that Eq. (17) is independent of $\delta \varphi / \delta b_n$. On the cavity boundary a non-homogeneous Neumann condition is to be satisfied.

$$\Delta \psi = 0, \quad (x, y) \in \Omega, \tag{19}$$

$$\nabla \psi \cdot \mathbf{n} = 0, \quad (x, y) \in \Gamma_{wetted}, \tag{20}$$

$$\nabla \psi \cdot \mathbf{n} = \rho \nabla_s \; V_t(p - p_v) \; , \quad (x, y) \in \Gamma_c. \tag{21}$$

Since the admissible shapes of the cavity shape are such that s_D, s_L are fixed, the variation $\delta \varphi / \delta b_n$ at these positions along the boundary are zero. The only problem arises when we try to define the pressure attenuation region TL. In our formulation the position of s_T should be such that $V_t = U_\infty \sqrt{\sigma + 1}$, equivalently $p = p_v$. For that reason, we assume that the term in Eq. (17) associated with s_T is also zero. However, the length of the pressure attenuation region is included in the set of design variables. The undefined constant associated with the exterior Neumann boundary value problem Eqs. (19-21) is resolved, in the present work, by assuming $\psi(t_o) = 0$. The latter is used in conjunction with continuity assumption of the adjoint potential ψ, thus dropping the last two terms in the right hand-side of Eq. (17).

3 NUMERICAL IMPLEMENTATION

3.1 Solution of the primal problem

For the solution of the primal problem in Eq. (5-8), a low order panel method based on piece-wise constant source and vortex distributions is implemented; see [10]. The boundary is approximated with N straight line segments denoted as panels and denoted as $\partial \Omega^h$. On each

panel the distribution of sources and vortices is piece-wise constant.

$$q(s)=q_j, \quad j=\ 1,N\ , \quad \gamma(s)=\gamma. \tag{22}$$

The total velocity $\mathbf{V}_i=\ u_i,\upsilon_i\ $ at the midpoint of the $i-th$ panel is given by

$$u_i=U_\infty^x+\sum_{j=1}^{N}q_j u_{sij}+\gamma\sum_{j=1}^{N}u_{vij}, \quad \upsilon_i=U_\infty^y+\sum_{j=1}^{N}q_j \upsilon_{sij}+\gamma\sum_{j=1}^{N}\upsilon_{vij} \tag{23}$$

with

$$u_{sij},\upsilon_{sij}\ =\int_{panel_j}\frac{x_{si},y_{si}}{2\pi r_{si}^2}ds, \qquad u_{vij},\upsilon_{vij}\ =-\int_{panel_j}\frac{-y_{si},x_{si}}{2\pi r_{si}^2}ds, \tag{24}$$

where $\mathbf{r}_{si}=\ x_{si},y_{si}\ $ is the relative position of the control point $\ \bar{x}_i,\bar{y}_i\ $ to the point of integration. Particularly $\ x_{si}=\bar{x}_i-x_s,\ \mathrm{y}_{si}=\bar{y}_i-y_s$. The discretized form of the boundary conditions is as follows

$$\mathbf{V}_i\cdot\mathbf{n}_i=0, \quad i=\ 1,\ldots N\ , \tag{25}$$

$$\mathbf{V}_1\cdot\mathbf{t}_1+\mathbf{V}_N\cdot\mathbf{t}_N=0. \tag{26}$$

Based on the above Eqs. (25-26) we can form a system of $N+1$ equations with $N+1$ unknowns. These are the strengths of the vortex and source distributions respectively. The pressure coefficient at the midpoint of the $i-th$ panel can be calculated using

$$C_p\ \bar{x}_i,\bar{y}_i\ =1-\frac{V_{ti}^2}{U_\infty^2}, \tag{27}$$

where V_{ti} is the tangential velocity at the midpoint of each panel. For the lift and the moment coefficients we assume that C_p is constant on each panel.

To illustrate that the boundary element algorithm performs satisfactorily within the scope of potential theory, we present in Figure 2a, a comparison between the obtained $CL-a$ curve with experimental data found in [13] as well as simulations performed with the inviscid version of XFOIL [14] for a NACA4412 hydrofoil at angle of attack $a=4\mathrm{deg}$, free-stream velocity $\mathbf{U}_\infty=(1,0)$. Moreover, a convergence study for the same test case is presented in Figure 2b. The simulation with the finest discretization serves as the reference case.

3.2 Solution of the adjoint problem

The adjoint field equation accompanied with non-homogeneous Neumann type conditions can also be treated in the sense of boundary integral methods

$$\nabla^2\psi=0, \quad (x,y)\in\Omega, \tag{28}$$

$$\nabla\psi\cdot\mathbf{n}=0, \quad (x,y)\in\Gamma_{wetted}, \tag{29}$$

$$\nabla\psi\cdot\mathbf{n}=\rho\nabla_s\ V_t(p-p_v)\ ,\quad (x,y)\in\Gamma_c. \tag{30}$$

The same discretization scheme is used to approximate the boundary of the foil including the cavity surface. Since this problem does not have circulation, vortex elements are not used in the representation and on each panel the distribution of sources is piece-wise constant, $\sigma(s)=\sigma_j,\quad j=\{1,\ldots N\}$. The adjoint velocity $\mathbf{V}_{ai}=\ u_{ai},\upsilon_{ai}$ at the midpoint of the $i-th$ panel is given by

$$u_{ai}=\sum_{j=1}^{N}q_j u_{sij},\quad \upsilon_{ai}=\sum_{j=1}^{N}q_j\upsilon_{sij}, \tag{31}$$

with u_{sij},υ_{sij} defined in Eq. (24). The boundary conditions in discretized form are

$$\begin{aligned}\mathbf{V}_{ai}\cdot\mathbf{n}_i&=\rho\partial_s\ V_{ti}(p_i-p_v)\ , && (\bar{x}_i,\bar{y}_i)\in\Gamma_c\\ &=0, && (\bar{x}_i,\bar{y}_i)\in\Gamma_{wetted}\end{aligned} \tag{32}$$

with the directional derivative on the *rhs* evaluated using a finite difference scheme. Based on the above Eq. (32) we can form a system of N equations with N unknowns. These are the strengths of the piece-wise constant source distributions σ_j.

To further illustrate the quantitative differences between the primal and the adjoint solutions we present in Figure 3 results obtained with the present method, for the case of a NACA16006 hydrofoil at $a=4\text{deg}$, $\mathbf{U}_\infty=(1,0)$ with an attached cavity. The cavity shape in this example is merely an initial guess for the test case presented in the section that follows. Particularly, the cavity length is set equal to $l_c/c=0.5$. In Figure 3a, we present the non-dimensional pressure field around the foil along with the disturbance velocity streamlines obtained for a non-cavitating foil with the fully wetted algorithm (primal problem). In Figure 3b, we present the corresponding adjoint potential field and the adjoint velocity streamlines.

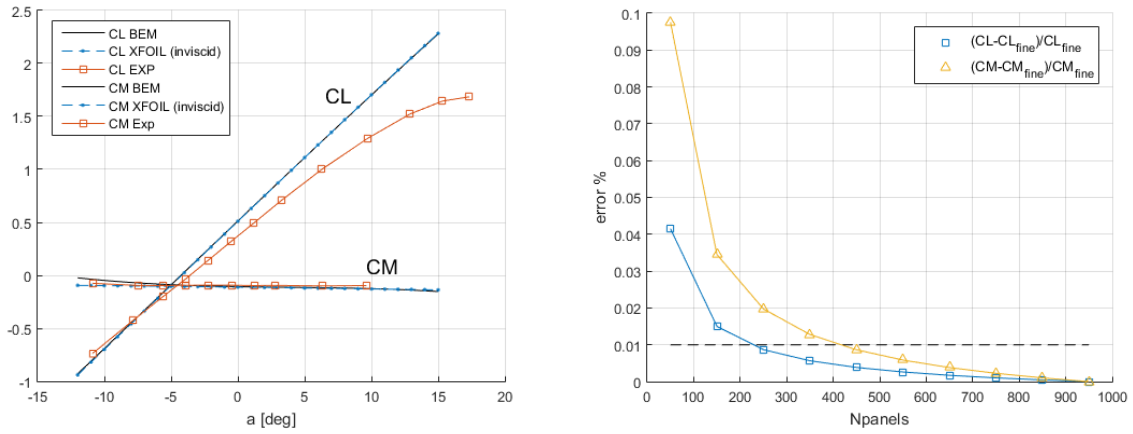

Figure 2. Numerical results for the NACA0012 hydrofoil. **(a)** Comparison between the present method and experimental data found in [13] as well as inviscid simulations using XFOIL [14]. **(b)** Convergence study for the primal solver.

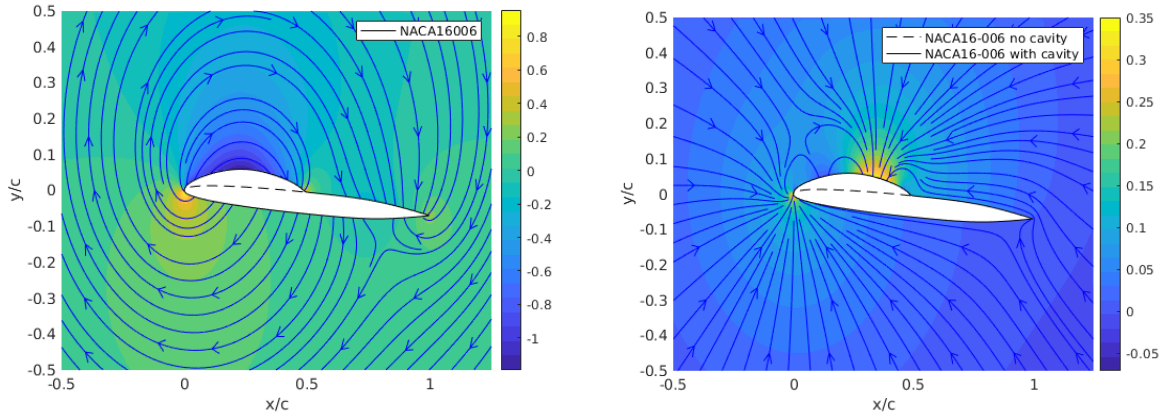

Figure 3. Numerical results for the NACA16-006 hydrofoil at α=4deg. **(a)** Pressure coefficient and disturbance velocity field streamlines. **(b)** Adjoint potential ψ and velocity streamlines.

3.3 Optimization algorithm

Our analysis leads to the algorithm (PCAVOPTIM) described below. Since the simple steepest-descent method is implemented, the rate of convergence is strongly dependent on the selection of the constants η, as well as the initial guess for the design variable vector. The optimization process continues until the solution has converged or the number of maximum evaluations $\mathrm{M}_{\max}$ has been reached. To verify that the proposed method is capable of predicting the sensitivity derivatives we performed comparisons with results obtained using a central difference scheme with fine discretization. In Figure 4a we assume that s_D is known and introduce $N = 24$ degrees of freedom. The results are in good agreement with the central differences in terms of order of magnitude and sign.

Algorithm 1: PCAVOPTIM

Initialize $b_n^0 = \{1, ..., N\}$ and set $\eta > 0, M_{max}$
while $M_{optim} < M_{max}$ **do**
  Solve primal problem to define ϕ
  Solve adjoint problem to define ψ
  Calculate sensitivity derivative $SD = \delta L / \delta b_n$
  Update $b_n^{k+1} := b_n^k - \eta \cdot (\delta L / \delta b_n^k)$
  Update $k = k + 1$
  Update $M_{optim} = M_{optim} + 1$
end while
return b_n^{k+1}

The cavity initialization affects the sensitivities near the edges of the cavity and this is observed especially for the $\delta L / \delta x_i$ sensitivities. Assuming that the constants selected for the steepest-descend scheme are sufficiently small, a local optimum is reached as the design cycles progress. This is evident from the convergence study presented in Figure 5. Increasing

the total number of design variables from $N_{DOFS}=10$ to $N_{DOFS}=30$ improves the final result, however, in the case of $N_{DOFS}=40$ over-fitting interferes with the final result.

3.4 Numerical Results

To highlight the ability of the proposed numerical scheme to predict both the cavity shape and the cavitation number as part of the solution, we present a comparison with Kinnas et al. [3]. The cavitation shape corresponds to a NACA16006 hydrofoil at $a=4\deg$, cavity length $l_c/c=0.5$ and pressure attenuation region defined by $\lambda l_c=0.05$. The initial guess for the cavity boundary for all simulations is a parabolic arc and s_D is positioned at the leading edge. The parametrization of the final cavity shape in terms of control points is given Table 1, whereas the initial and final shape of the cavity are shown in Figure 6. The pressure coefficient distribution is in excellent agreement with the model presented in [3] based on the results obtained with the PCAVOPTIM shown in Figure 7. The cavity volume or more precisely the sectional area is also of great interest, since in an unsteady case changes in volume determine the monopole-type acoustic source strength. The proposed model is able to predict the volume of the cavity and particularly for the case study in [3] with 2% accuracy.

Table 1: Attached cavity B-spline control points

cp_n	x_i	y_i	cp_n	x_i	y_i
1	0	0	9	0.317714202	0.07419988
2	-0.000003922	0.002778050	10	0.379138102	0.07248445
3	0.005049522	0.009740524	11	0.432027052	0.06650745
4	0.031419923	0.025242150	12	0.476973355	0.05536975
5	0.071704606	0.039947408	13	0.499050602	0.03302545
6	0.124515013	0.053675617	14	0.501870332	0.02999972
7	0.185911923	0.064407361	15	0.503675578	0.02999959
8	0.251802936	0.07146618		……	……

4 CONCLUSIONS

The problem of steady, partially cavitating two-dimensional hydrofoils is formulated in a shape-optimization setup. In terms of the cavity shape, the control points of the B-spline cavity parametrization are included in the set of design variables. The problem is solved by implementing an optimization algorithm using the continuous adjoint method to calculate the sensitivity derivatives. The proposed numerical scheme when compared with other methods and data from a numerical test case and is found to predict well the cavity shape, volume and cavitation number. Finally, the benefits of using the adjoint method to predict the sensitivity derivatives, in comparison to the standard finite difference scheme followed in the gradient method are discussed.

Future work is planned towards systematic comparisons with experimental data and other methods as well as the investigation of the effects of camber and thickness on cavity shape and volume. Treatment of the ‘direct problem’ as addressed in [3], where the cavitation number is known and the cavity shape and length are to be determined upon solution of the

problem, is a challenging variation left for future work. Finally, the present model could be extended to treat the problem of cavitating hydrofoils operating beneath the free-surface.

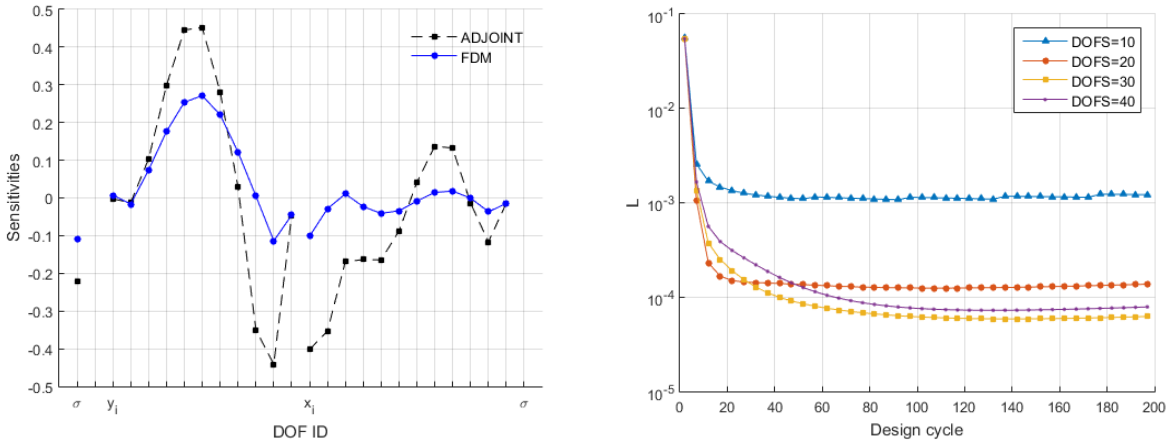

Figure 4. PCAVOPTIM **(a)** Comparison between the sensitivities obtained using the proposed method and a finite difference scheme. **(b)** Convergence study for the cost functional during each design cycle with the total number of design variables as a parameter.

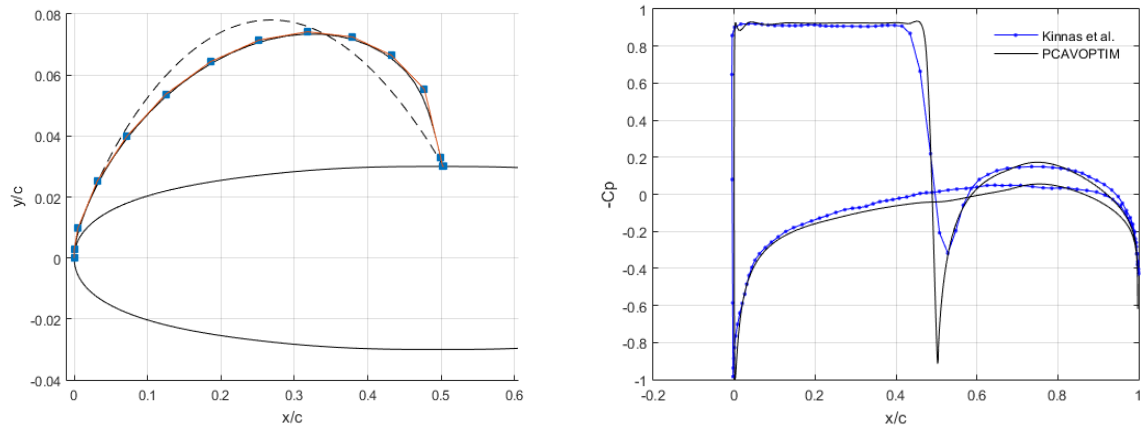

Figure 5. Comparison between the present method and results found in Kinnas et al [3]. **(a)** Initial and final cavity shape for the partially cavitating NACA16006 foil with $l_c / c = 0.5$ at $a = 4\text{deg}$. Cavity characteristics $\sigma = 0.92$, $h_{\max} / c = 0.073486$, $Vol / c^2 = 0.01366$. The squares represent the control points of the B-spline representation. **(b)** Pressure coefficient for the partially cavitating NACA16006 and comparison with [3].

REFERENCES

[1] Leroux, J.B., Coutier-Delgosha, O. and Astolfi, J.A., A joint Experimental and Numerical Study of Mechanisms associated to Instability of Partial Cavitation on Two-dimensional Hydrofoils. *Physics of Fluids* (2005) **17**:052-101.

[2] Uhlman, J., The Surface Singularity Method Applied to Partially Cavitating Hydrofoils. *Journal of Ship Research* (1987) **31**:107-124.

[3] Kinnas, S. and Fine, N.E., A Numerical Nonlinear Analysis of the Flow Around Two- and Three-Dimensional Partially Cavitating Hydrofoils. *J. Fluid Mech.* (1993) **254**:151-181.

[4] Lemonnier, H. and Rowe A., Another Approach in Modelling Cavitating Flows. *J. Fluid Mech.* (1988) **195**:557-580.

[5] Pironneau O., *Optimal shape design for elliptic systems*. Springer-Verlag, (1983).

[6] Choi, J., Penmetsa, R. and Grandhi, R. Shape Optimization of the Cavitator for a Super-cavitating Torpedo. *Structural and Multidisciplinary Optimization* (2005) **29**:159-167.

[7] He, P., Filip, G., Martins, J. and Maki, K., Design Optimization for Self-propulsion of a Bulk Carrier using a Discrete Adjoint Method. *Computers and Fluids* (2019) **192**:104-259.

[8] Papoutsis-Kiachagias, E., Kyriacou, S. and Giannakoglou, K., The Continuous Adjoint Method for the Design of Hydraulic Turbomachines, *Computer Methods in Applied Mechanics and Engineering* (2014) **278**:621-639.

[9] Boger, D. and Paterson, E., A Continuous Adjoint Approach to Design Optimization in Cavitating Flow using a Barotropic Model. *Computers and Fluids* (2014) **101**:155-169.

[10] Morlando, F., Adjoint-based Sensitivity Analysis by Panel Methods and CAS. *Optimization Letters* (2017) **11**:739-752.

[11] Moran J., *An introduction to theoretical and computational aerodynamics*, John Wiley & Sons (1984).

[12] Gelfand, I.M. and Fomin, S.V., *Calculus of Variations*. Prentice-Hall Inc., Englewood Clifs, New Jersey, (1963).

[13] Abbott, I., Doenhoff, A., *Theory of Wing Sections,* Dover Publications, Inc., (1959).

[14] Drela, M., An analysis and design system for low Reynolds number Airfoils. In: Mueller T.J. *Low Reynolds Number Aerodynamics. Lecture Notes in Engineering* Springer, Berlin, Heidelberg, Vol.54 (1989).